Influence of the shape of mitigation barriers on heavy gas dispersion

V. Busini*, R. Rota

Department of Chemistry, Materials and Chemical Engineering "G. Natta", Politecnico di Milano, Piazza Leonardo da Vinci 32, Milano, Italy

Received 25 September 2013
Received in revised form
19 December 2013
Accepted 8 January 2014

1. Introduction

Regasification plants have become an emerging risk because their numbers are increasing and concern from the general population towards these systems has grown. Thus, the risks associated with the storage and transportation of liquefied natural gas (LNG) have been a highly discussed topic in the literature in recent years. In particular, the need to assess this risk has given rise to several studies carried out with both simulation models and experiments on large-scale spills of LNG (Luketa-Hanlin, 2006). A good collection of potential hazards related to handling LNG and techniques to model and analyze the consequences of these hazards is contained in a recent book by Woodward and Pitblado (2010) and in a paper by the same authors (Pitblado & Woodward, 2011; Woodward & Pitblado, 2010).

Moreover, accident histories compiled by Delano (2003), Bainbridge (2003), and LNG World Shipping (2006) reveal that most accidents over the last 50 years happened during operation of the LNG carrier at the dock or inside the plant; these locations are complex environments characterized by the presence of large obstacles (Bainbridge, 2003; Delano, 2003; LNG World Shipping, 2006). This poses the problem of how to define the adequacy of available models for the study of LNG dispersion in real conditions (Ivings, Jagger, Lea, & Weber, 2007) and, more generally, of the dispersion of dense gases in the presence of large obstacles such as real and complex industrial geometries. Several works indeed stress that the common practice is to use integral models, which, on the other hand, are intrinsically unable to include the presence of obstacles because their predictions are realistic and reliable only under open-field conditions (Witlox, Harper, & Pitblado, 2013). Neglecting the effect of large obstacles (such as physical barriers) to the dispersion of dense gases can lead to macroscopic errors (Britter, 1998; Nielsen, 1998). To evaluate the dispersion of dense gases in complex environments, it is therefore necessary to use models developed in the frame of computational fluid dynamics (CFD) as discussed in several works in the literature (Busini et al., 2011; Gavelli, Bullister, & Kytomaa, 2008; Gavelli, Chernovsky, Bullister, & Kytomaa, 2010; Koopman & Ermak, 2007; Luketa-Hanlin, Koopman, & Ermak, 2007; Pontiggia, Busini, Gattuso, Uguccioni, & Rota, 2012; Pontiggia et al., 2010; Tauseef, Rashtchian, & Abbasi, 2011; Zhang, Ning, & Ma, 2009). These models allow the evaluation of obstacle effects (e.g., the size and shape of eddies or the interaction between vortices caused by nearby obstacles) in order to implement simplified formulas in integral models (Scaperdas & Hebden, 2003) or to evaluate the effect of mitigation barriers on the expected hazardous distance (Busini, Lino, & Rota, 2012). In particular, the influence of mitigation barriers on atmospheric dispersion has been an active topic of research in the field of street canyons (Hagler et al., 2012).

In this work, computational fluid dynamics models were used to analyze the performance of mitigation barriers with different shapes. In particular, we employed a case study similar to another recent work that analyzed the effect of simple mitigation barriers on the dispersion of an LNG gas cloud in a regasification terminal (Busini et al., 2012). Our goal was to probe the effects of different barrier characteristics (e.g., roughness, battlements, and holes). The

* Corresponding author. Tel.: +39 02 2399 3186.
E-mail address: valentina.busini@polimi.it (V. Busini).

final aim was to improve dense gas dispersion by increasing the turbulence level behind the barrier and, therefore, the mixing rate between air and the gas cloud.

2. Materials and methods

Computational fluid dynamics codes solve numerically and simultaneously the Navier–Stokes equations of motion, the energy balance and the equation arising from turbulence modeling (Launder & Spalding, 1972; Luketa-Hanlin, Koopman, & Ermak, 2007). The domain is discretized through the use of a calculation grid that allows transformation of the partial differential equations into a system of algebraic equations.

In this work, the k–ε model was used to represent the effects of the turbulence. This model was complemented with an Atmospheric Stability sub-Model (ASsM) that ensures the consistency of the CFD results with the Monin–Obukhov theory (Pontiggia, Derudi, Busini, & Rota, 2009).

The reliability of the CFD model used in all computations reported in this work has been previously verified by comparison with experimental measurements both in free-field conditions and in the presence of large obstacles (Pontiggia et al., 2009; Pontiggia et al., 2011).

The commercial package Fluent 12.1.2 (ANSYS Inc., 2009) was used for all computations together with the boundary conditions summarized in Table 1.

For the sake of comparison, the Process Hazard Analysis Software Tools (PHAST) software was also used (DNV, 1999). PHAST can examine the progress of a potential accident from the initial release to the far-field dispersion including modeling pool spreading and evaporation through integral models, which are unable to account for the presence of large obstacles as previously discussed.

To size the mitigation barrier, a previously developed criterion was used (Derudi, Bovolenta, Busini, & Rota, 2014); here, it suffices to mention that the dimensionless parameter R^* allows the characterization of different types of obstacle. Such a parameter is defined as the minimum between two other parameters: the ratio between the height of the frontal face of a given obstacle, h_{obs} (or width w_{obs}), and the cloud height h_{cld} (or cloud width w_{cld}) evaluated under free-field conditions (that is, without any obstacles):

$$R_h = \frac{h_{obs}}{h_{cld}} \tag{1}$$

$$R_w = \frac{w_{obs}}{w_{cld}} \tag{2}$$

$$R^* = \min(R_h, R_w) \tag{3}$$

It has been shown that an obstacle's influence on the hazardous distance can be disregarded for $R^* < 0.25$ while it must be considered for $R^* > 1$. The range $0.25 < R^* < 1$ represents a sort of transition zone where the influence of the obstacle cannot be foreseen (Derudi et al., 2014). Therefore, an effective mitigation barrier should be characterized by a value of $R^* \geq 1$.

Table 1
Boundary conditions.

Ground	Wall @ 300 K, roughness = 0.06 m
Walls	Adiabatic wall, roughness = 0.005 m
Pool	During atmospheric stabilization: Wall @ 300 K, roughness = 0.01 m During pool evaporation: mass flow inlet After the end of pool evaporation: adiabatic wall
Wind inlet, domain sides, sky	Velocity inlet
Wind outlet	Pressure outlet

3. Results and discussion

As a case study, a release of LNG deriving from the full-bore rupture of a pipeline was selected. The characteristics of both the pipeline and storage are reported in Table 2.

The modeling of the LNG dispersion was performed for a 5D stability class and 5 m/s wind speed at 10 m above the ground with the suite package PHAST to define the pool dimensions deriving from the spill and the evaporating mass flow; the results of this simulation in terms of vaporization rate are shown in Fig. 1 while the lower part of Fig. 2 illustrates the maximum distance at which the LNG concentration reaches the lower flammability limit (LFL). This distance is not representative of a specific time after the start of the release; rather, it shows the area where hazardous concentration values larger than the LFL are expected. According to Fig. 2, PHAST predicts that the cloud takes an elongated shape typical of dense gas releases with a fair amount of spreading in the initial part and a progressive narrowing up to dissipation; the maximum distance reached by the cloud is approximately 570 m from the center of the pool. These results are expected to be reliable in the absence of large obstacles because PHAST has been successfully validated in comparison with experimental data obtained in the open field.

This pre-modeled source term was used in the CFD simulations by considering a pool with a radius of 5 m and a mesh built using GAMBIT (ANSYS Inc., 2004) size functions to make the grid denser in critical areas; the size of the domain of integration was $1000 \times 50 \times 800$ m.

To simulate the initial expansion and the subsequent shrinkage of the pool, the boundary conditions of the surface, which were initially set as *wall* with the same characteristics as the terrain during the first phase of wind stabilization, were changed to *mass flow inlet* and then *adiabatic walls*.

The CFD results obtained under open field conditions are compared with those of the integral model in Fig. 2 where the upper part shows projections of the LFL contour on the ground obtained with two different grid sizes ($7 \cdot 10^4$ cells and $4 \cdot 10^6$ cells). We can see that the results obtained with the larger number of cells are in fair agreement with those obtained with the smaller number of cells; therefore, proving that the computed hazardous distance is reasonably grid independent. As in the PHAST simulation, the cloud develops mainly along the wind direction even if the spreading is less significant and the narrowing takes place less gradually, which leads to a more abrupt edge of the cloud. The maximum distance reached by the cloud is approximately 520 m from the center of the pool, which is in reasonable agreement with the value predicted by PHAST.

The open-field CFD simulation also evaluated the height of the cloud. Based on the results, the necessary height of the mitigation barrier can be estimated as approximately 6–7 m tall using the aforementioned constraint $R^* = 1$ (see Fig. 2B).

For all the shapes investigated, the mitigation barrier was positioned at 150 m from the pool's center and was 450 m wide (in

Table 2
Characteristics of both pipeline and storage.

Pipe diameter	1 m
Total inventory	45,000 kg
Temperature	111 K
Pipeline length	20 m
Density	450 kg/m^3

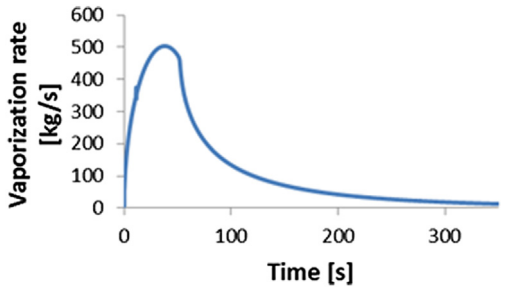

Fig. 1. Source term computed with PHAST and used in the CFD simulations.

order to contain thoroughly the entire width of the cloud) with a thickness of 0.5 m.

Because one of the main characteristics of cold dense clouds is their tendency to reduce turbulence and gravity flow along with the effects of terrain and obstacles (Koopman, Ermak, & Chan, 1989), the rationale with which the mitigation barriers were designed, was to induce a larger increment of the turbulence. Five different shapes were simulated:

- Simple walls with different heights and roughnesses.
- Crenellated walls, which should induce vortexes and wakes at the top of the barrier where the cloud overcomes the barrier.
- Perforated walls, which should divide the cloud into several small jets entraining clean air behind the barrier.
- Multiple staggered walls, which should channel the cloud into several aisles towards the clean air behind the barrier.
- Tilted walls, which should rotate the cloud movement to flow upwind.

Full details about the various geometries are given in the following dedicated paragraphs.

3.1. Simple walls

Three different simple walls were simulated:

- Wall S1: 6 m high and 450 m wide.
- Wall S2: 7 m high and 450 m wide.
- Wall S3: 6 m high and 450 m wide with roughness of 0.1 m.

The first two walls were used to verify that an obstacle characterized by $R^* \geq 1$ strongly influences the hazardous distance. Wall S3 was used to determine the influence of the roughness of the wall on the local turbulence.

As shown in Fig. 3, all three walls are effective, which validates the aforementioned criterion (Derudi et al., 2014). The walls caused a reduction of the distance reached by the LFL (with respect to the open-field case) equal to 43% for the S1 and S3 walls and 63% for the S2 wall. While increasing the barrier height from 6 to 7 m leads to an increase in the mitigation efficiency, incrementing the wall roughness does not influence the downwind distance reached by the LFL. This means that even a large increase in the roughness of the wall will not be able to significantly influence the turbulence of the cloud.

Considering its significant reduction of 43%, wall S1 was taken as the base case for comparison with the other barriers.

3.2. Crenellated walls

The effectiveness of the replacement of the upper part of the wall with a crenellation was investigated with the goal of obtaining a higher production of local turbulence around the battlements due to recirculation of the fluid in the horizontal direction.

Three configurations were investigated all characterized by wall heights of 6 m and widths of 450 m:

- Wall C1: dense battlements were inserted on the top of the wall (spaced 0.5 m apart with heights and widths of 0.5 m);
- Wall C2: sparse and wider battlements were inserted on the top of the wall (spaced 2 m apart with heights of 0.5 m and widths of 5 m);
- Wall C3: taller battlements were inserted on the top of the wall (spaced 1 m apart with heights of 1 m and widths of 15 m).

The results shown in Fig. 4 suggest only a marginal influence for the changes implemented on top of the walls, in fact the hazardous distance in all cases was almost equal to that found in the base case S1 (simple uncrenellated wall). The limited benefit of the battlements is probably due to the massive amount of LNG released, which leads to the formation of a cloud with considerable inertia that can hardly be influenced by small-scale obstacles such as battlements.

This is illustrated in Fig. 5 where the contours of the turbulent intensity around the different walls are sketched both with and without the cloud hitting the wall. Before the arrival of the cloud, the presence of the walls has a strong influence on the turbulence level both for simple walls (Fig. 5a) and crenellated walls (Fig. 5c); upon arrival of the cloud, turbulence decreases dramatically (see

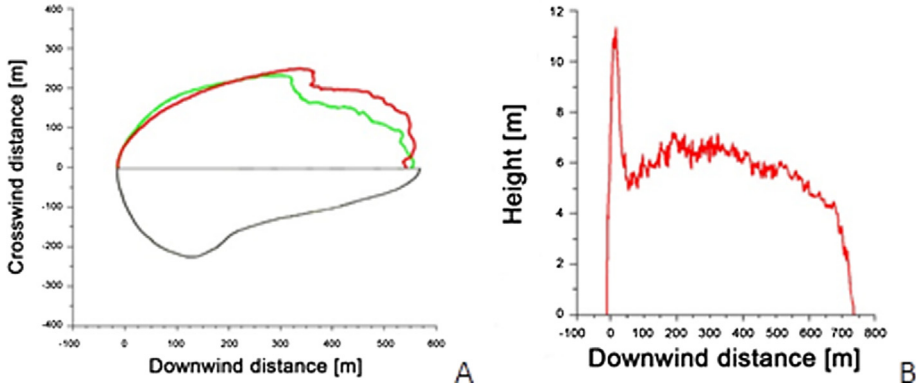

Fig. 2. A) Maximum LFL footprint in open-field conditions: the upper part reports CFD model predictions obtained with $7 \cdot 10^4$ cells (green/light line) and $4 \cdot 10^6$ cells (red/dark line); the bottom part reports predictions of the integral model. B) Cloud height profile at LFL along the wind direction, in correspondence of domain symmetry plane, predicted by the CFD model. (For interpretation of the references to color in this figure legend, the reader is referred to the web version of this article.)

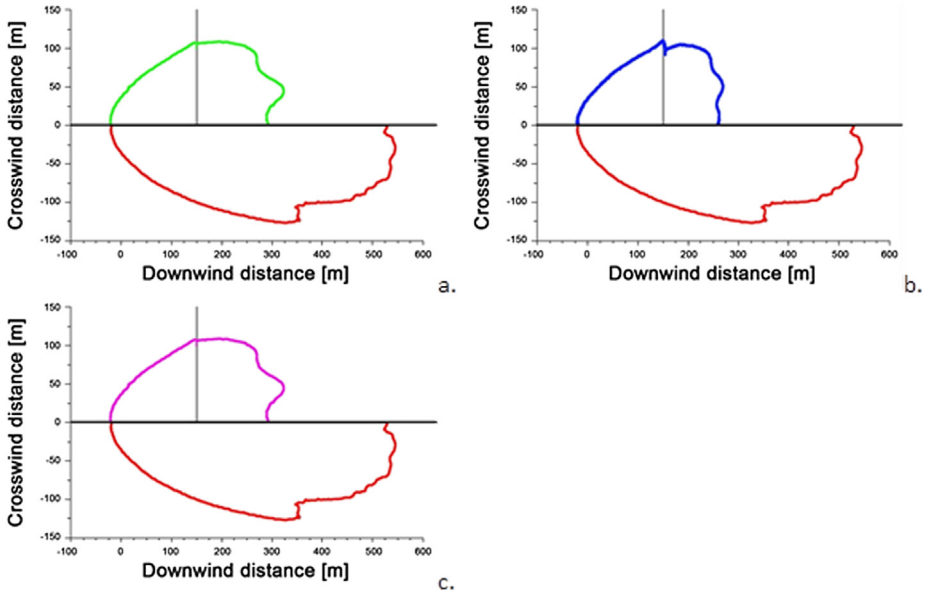

Fig. 3. Upper part: downwind distance reached by the LFL for walls S1 (a), S2 (b), and S3 (c); lower part: downwind distance reached by the LFL in the open-field simulation.

Fig. 5b for simple walls and Fig. 5d for crenellated walls) and almost no differences are evident between simple and crenellated walls. Fig. 5 reports the results only for wall C1 as it is representative of the other types of crenellated walls.

3.3. *Perforated walls*

Mitigation barriers containing vertical slits of different sizes were simulated with the aim of inducing the formation of cloud jets from the fissures that would promote the mixing and dispersion of the LNG cloud with the air behind the fissures.

Three configurations were investigated all characterized by wall heights of 6 m:

- Wall P1: vertical holes (dimensions 0.5 × 0.5 × 4.5 m) were inserted with 1 m spacing at 1 m from the ground;
- Wall P2: higher vertical holes (dimensions 0.5 × 0.5 × 2 m) were inserted with 1 m spacing at 2.5 m from the ground; and

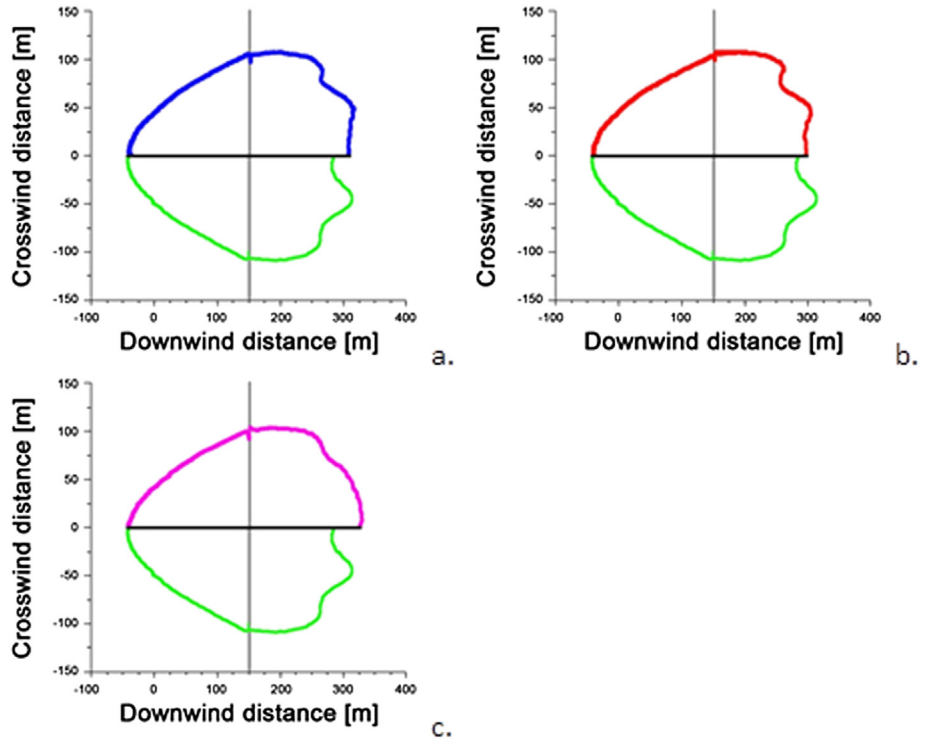

Fig. 4. Upper part: downwind distance reached by the LFL for walls C1 (a), C2 (b), and C3 (c); lower part: downwind distance reached by the LFL for the simple wall S1.

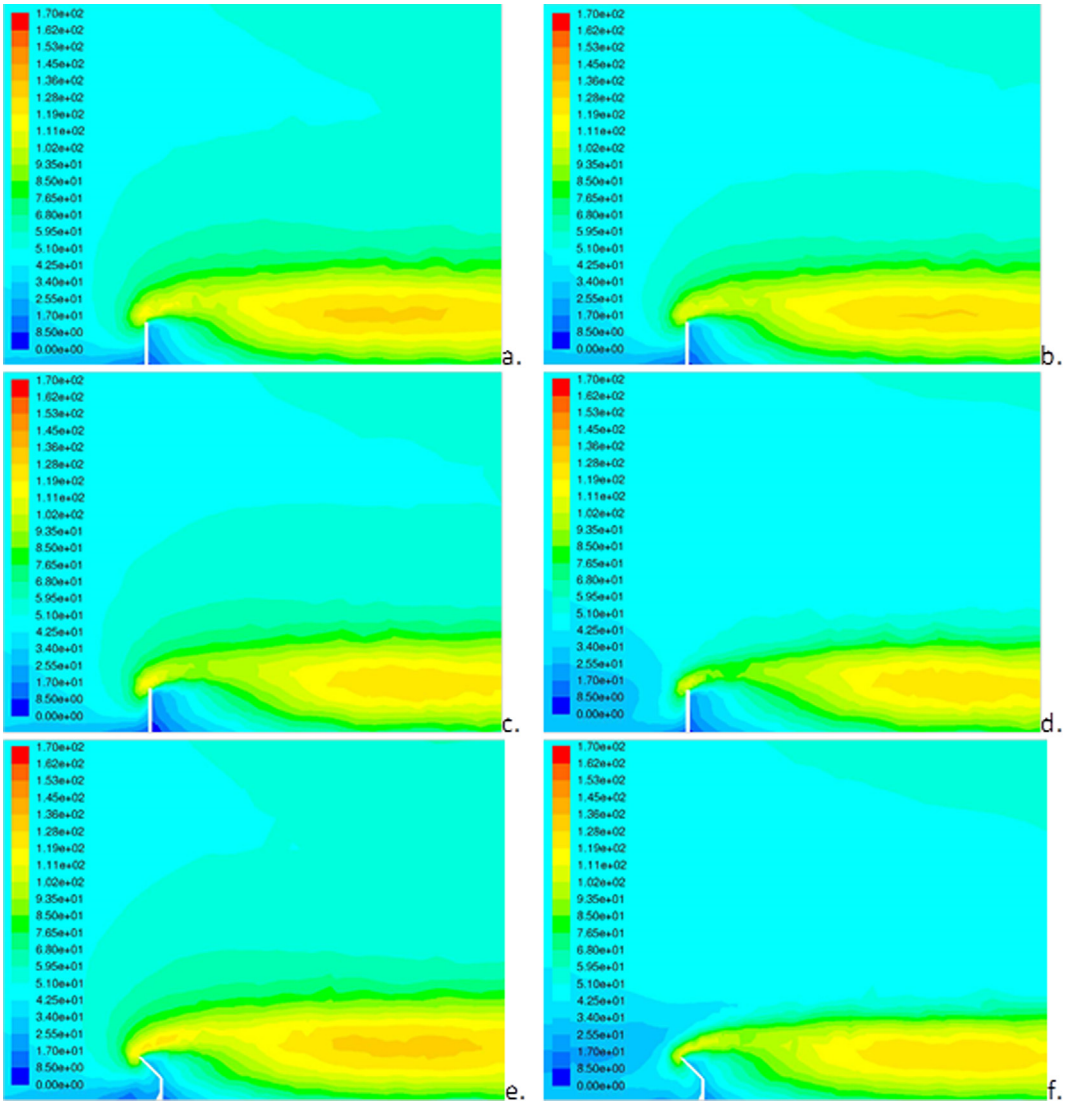

Fig. 5. Contours of turbulent intensity [%] without (a) and with (b) the cloud of LNG for the simple wall S1; without (c) and with (d) the cloud of LNG for the crenellated wall C1; and without (e) and with (f) the cloud of LNG for the tilted wall T4.

- Wall P3: less dense vertical holes (dimensions 0.5 × 0.5 × 2 m) were inserted with 2 m spacing at 2.5 m from the ground.

As can be seen from the cloud footprints reported in Fig. 6, the barriers in this case are also unable to significantly change the hazardous distance with respect to the base case. The poor performance of vertical slits can be ascribed on one hand to the massive amounts of natural gas involved in the release, which overcame the effect of barrier mixing due to the relatively low amount of LNG passing through the hole; on the other hand, the formed clouds have considerable inertia, and they are hardly influenced by small changes to the base barrier case (as in the crenellated wall case).

Therefore, these results confirm the inability of small changes in the barrier's geometry to affect the turbulence of heavy cold clouds and suggest that the efficacy of the barrier is more simply related to the barrier's hindrance to downwind cloud dispersion. The efficiency, for simple, crenellated and perforated walls, can be related to the effective hindrance area through a hindrance parameter, *E*, defined as the following:

$$E = \frac{(\text{full Area} - \text{blank Area})}{(\text{full Area})_{\text{BaseCase}}}$$

where (full Area − blank Area) is the area of the wall on which the cloud will impact minus the area subtract from the wall by holes and battlements and $(\text{full Area})_{\text{BaseCase}}$ is the area of the base case S1, which is equal to 2700 m^2.

Table 3 summarizes the values of the parameter *E* for all of the investigated configurations, and Fig. 7 shows the correlation between this parameter and the barrier efficiency in terms of the hazardous distance. We can see that the data are linearly correlated with a value of $R^2 = 0.92$ and a Pearson correlation coefficient, ρ_{xy}, equal to −0.96. This correlation highlights that the only relevant mitigation effect for these barriers is related to the physical hindrance presented by the walls because they are not able to significantly alter the low turbulence values induced by the cold cloud.

3.4. Multiple staggered walls

The previous attempts to enhance the turbulence level (and, therefore, the mixing rate between cloud and air) through small

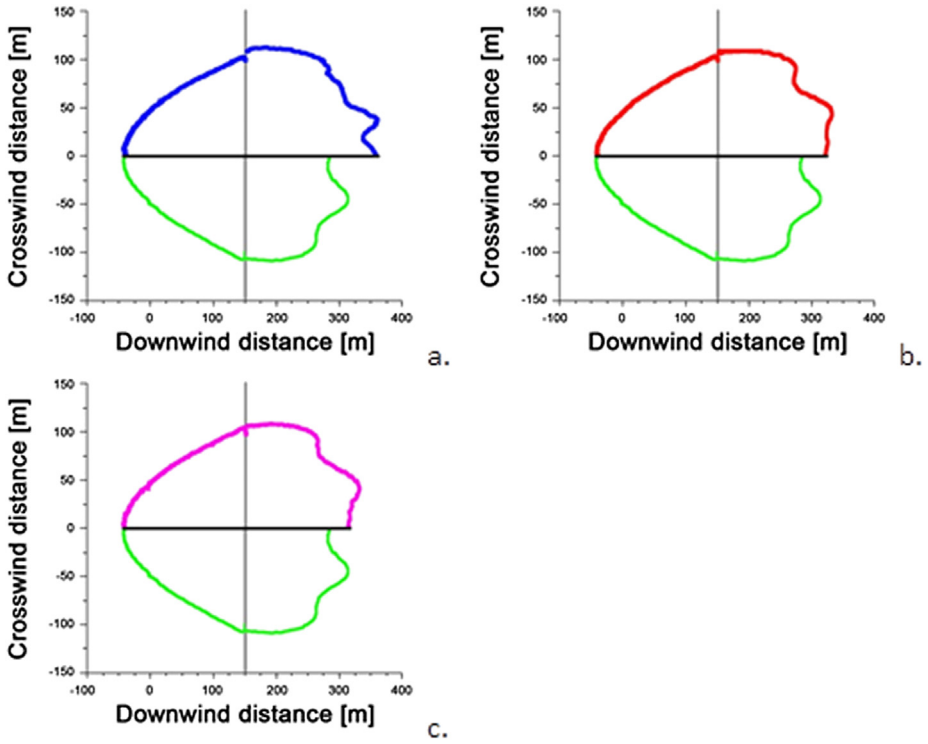

Fig. 6. Upper part: downwind distance reached by the LFL for walls P1 (a), P2 (b), and P3 (c); lower part: downwind distance reached by the LFL for the simple wall S1.

Table 3
Mitigation effectiveness of the various barriers investigated.

Case	Downwind distance (from the barrier position) reached by LFL	Variation (with respect to the base case S1) of the LFL distance from the barrier position	Downwind distance (from the pool center) reached by LFL	Variation (with respect to the open-field) of the LFL distance from the pool center	Hindrance parameter
S1 (base)	167 m	–	317 m	−44%	1
S2	127 m	−24%	277 m	−51%	1.17
S3	167 m	0%	317 m	−44%	1
C1	170 m	+2%	320 m	−44%	0.96
C2	169 m	+1%	319 m	−44%	0.94
C3	177 m	+6%	327 m	−43%	0.92
P1	220 m	+32%	370 m	−35%	0.81
P2	185 m	+11%	335 m	−41%	0.92
P3	188 m	+13%	338 m	−41%	0.94
M1	177 m	+6%	327 m	−43%	–
M2	208 m	+25%	358 m	−37%	–
M3	186 m	+11%	336 m	−41%	–
T1	150 m	−10%	300 m	−47%	–
T2	155 m	−7%	305 m	−46%	–
T3	155 m	−7%	305 m	−46%	–
T4	142 m	−15%	292 m	−49%	–

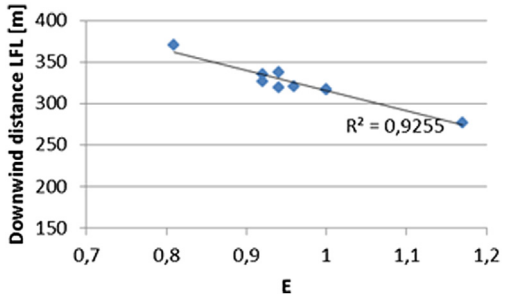

Fig. 7. Efficiency of the mitigation barriers in terms of hazardous distance vs. the hindrance parameter.

modifications of the base case barrier were not successful; therefore, the effect of a much more radical change in the barrier configuration was investigated by using multiple staggered walls. The concept is that the canalization of the cloud through several aisles towards the clean air behind the barrier could enhance the mixing rate between the air and the cloud and reduce the hazardous distance.

Three configurations were investigated all characterized by maintaining the staggered walls 6 m high with the rear row of walls spaced at 1 m and staggered to overlap by 1 m with the front wall:

- Wall M1: 5 walls were inserted (size 96 × 0.3 m);
- Wall M2: 16 walls were inserted (size 30 × 0.3 m); and

- Wall M3: 46 walls were inserted (size 10 × 0.3 m).

The dispersion of the cloud is sketched in Fig. 8 and is always represented in terms of the LFL footprint compared with the base case S1. We can see that the use of multiple staggered walls can worsen the situation with respect to the simple wall by increasing the LFL of the cloud to values above 350 m in the *x* direction.

The canalizations of the cloud through the walls did not force increased mixing but instead led to the formation of preferential passages for the cloud and limited the physical hindrance of the walls; this effect can be argued from the very jagged shape of the clouds (Fig. 9b in particular).

Table 3 summarizes all of the results in terms of the hazardous distance reached by the cloud beyond the barrier with respect to the base case. We can see that, in most cases, the use of walls with complex geometries does not improve the efficiency of the mitigation barrier in terms of the LFL distance. As previously discussed, this marginal effect should be ascribed to turbulence suppression induced by the cold cloud, which cannot be superseded by the additional vortices and wakes created by the various barrier modifications investigated. In all cases, the barrier acts mainly as an obstacle that must be overcome by the cloud, which behaves like a liquid. Therefore, the main effect of the barrier is to hinder the cloud path by forcing the cloud to move upward or spread laterally to overcome the barrier. During these movements, mixing with the surrounding air (with reference to the free-field situation) increases and the hazardous distance decreases.

As a consequence, the reduction of the hazardous distance induced by a mitigation barrier (at least for the passive barriers investigated in this work) should be mainly ascribed to changes in cloud movement rather than in any significant change to the mixing rate between cloud and air. Based on this conclusion, one last type of barrier was investigated in an attempt to reverse the cloud's path by forcing it to move upwind through tilted barriers as discussed in the following subsection.

3.5. Tilted walls

In this last case, a macro-recirculation of the fluid was induced upwind by using tilted barriers whose main expected effect is to reverse the cloud pattern upwind.

The four barriers investigated have a bottom part that is inclined downwind (1 m high for all configurations), a central straight part of variable length to achieve a total barrier height of 6 m, and a top part inclined upwind at different angles from the vertical:

- Wall T1: characterized by a central vertical part 4 m long and a top angle from the vertical of 45°;
- Wall T2: characterized by a central vertical part 4 m long and a top angle from the vertical of 63°;
- Wall T3: characterized by a central vertical part 4.5 m long and a top angle from the vertical of 63°; and
- Wall T4: characterized by a central vertical part 4.24 m long and a top angle from the vertical of 45°.

All of the tilted barriers demonstrated a reduction of the hazardous distance with respect to the base case as shown in Fig. 9 and Table 3.

In fact, even though the presence of the cold dense cloud reduces the turbulence intensity close to the wall (Fig. 5e and f), the large upwind vortices formed on top of the barrier, which reverse the cloud pattern, increase the downwind cloud dilution. The large vortices that are formed can be seen in Fig. 10, which shows the velocity field in the proximity of walls T4 and S1, the latter being the base case.

4. Conclusions

The main goal of this work was to investigate the effectiveness of mitigation barriers with different shapes on the dispersion of

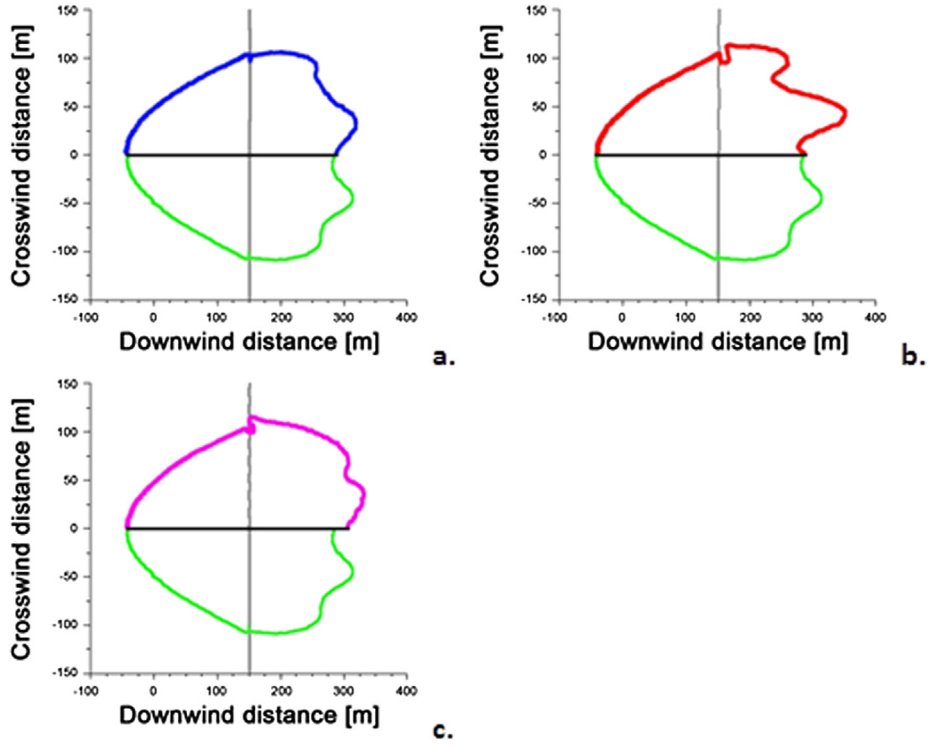

Fig. 8. Upper part: downwind distance reached by the LFL for walls M1 (a), M2 (b), and M3 (c); lower part: downwind distance reached by the LFL for the simple wall S1.

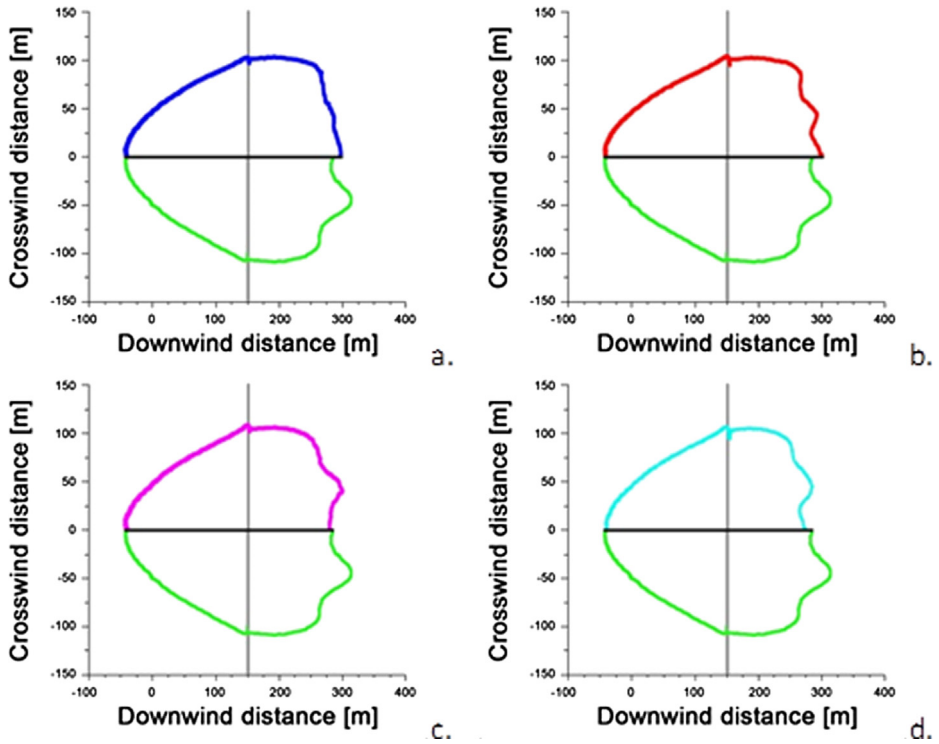

Fig. 9. Upper part: downwind distance reached by the LFL for walls T1 (a), T2 (b), T3 (c), and T4 (d); lower part: downwind distance reached by the LFL for the simple wall S1.

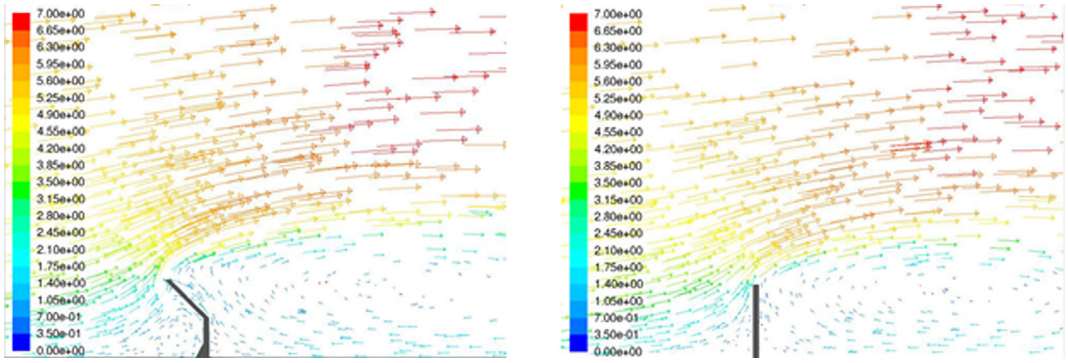

Fig. 10. Velocity field for barriers T4 (left) and S1 (right).

clouds produced by a massive release of a cold dense gas, namely, LNG. The effectiveness was evaluated in terms of hazardous distance, which is defined as the maximum downwind distance reached by the lower flammability limit.

It was found that attempts to increase the mixing rate between cloud and air through an increase of the turbulence level close to the barrier were almost completely ineffective; this was most likely due to the massive amount of LNG released, which leads to a cloud with remarkable inertia whose turbulence is hardly influenced by small changes in the barriers' structure such as battlements or holes.

These simulations permitted us to determine the relation between the abatement performance of various barriers and a geometrical parameter of the walls, namely, the hindrance parameter. Such a parameter relates almost linearly to the frontal area of a barrier that is acting as a physical obstacle to the cloud's progress and the hazardous distance reached by the cloud. This result indicates that the only relevant mitigation effect for these barriers is related to the physical hindrance represented by the walls because they are not able to significantly improve the low turbulence values induced by the cold cloud.

A more satisfactory result was obtained using tilted barriers, which were able to reduce the size of the cloud with respect to the base case. This effect is mainly due to mixing between air and the cloud induced by large vortices generated close to the inclined part of the top of the barriers; the vortices are able to reverse the cloud pattern and increase the downwind cloud dilution.

References

ANSYS Inc. (2004). *GAMBIT 2.2 tutorial guide* (Lebanon, NH, USA).
ANSYS Inc. (2009). *ANSYS Fluent 12 user's guide* (Lebanon, NH, USA).
Bainbridge, K. (2003). *An overview of the LNG shipping industry, fundamentals of base load LNG*. Linthicum, MD: Gas Tech. Institute Training Course.
Britter, R. E. (1998). *Recent research on the dispersion of hazardous materials*. EUR 18198 (p. 234). Luxembourg: Office for Official Publications of the European Communities.

Busini, V., Lino, M., & Rota, R. (2012). Influence of large obstacles and mitigation barriers on heavy gas cloud dispersion: a liquefied natural gas case-study. *Industrial & Engineering Chemistry Research, 51*(22), 7643–7650. http://dx.doi.org/10.1021/Ie201591b.

Busini, V., Pontiggia, M., Derudi, M., Landucci, G., Cozzani, V., & Rota, R. (2011). *Safety of LPG rail transportation*. In *Icheap-10: 10th International Conference on Chemical and Process Engineering, Pts 1–3, Vol. 24*; (pp. 1321–1326). http://dx.doi.org/10.3303/Cet1124221.

Delano, F. (2003). *Introduction to LNG* (p. 23). Houston, TX: Univ. of Houston Law Center, Institute for Energy, Law and Enterprise.

Derudi, M., Bovolenta, D., Busini, V., & Rota, R. (2014). Heavy gas dispersion in presence of large obstacles: selection of the modeling tools. *Industrial & Engineering Chemistry Research*. http://dx.doi.org/10.1021/ie4034895.

DNV. (1999). *PHAST 6.0 technical reference manual* (London, UK).

Gavelli, F., Bullister, E., & Kytomaa, H. (2008). Application of CFD (Fluent) to LNG spills into geometrically complex environments. *Journal of Hazardous Materials, 159*(1), 158–168. http://dx.doi.org/10.1016/j.jhazmat.2008.02.037.

Gavelli, F., Chernovsky, M. K., Bullister, E., & Kytomaa, H. K. (2010). Modeling of LNG spills into trenches. *Journal of Hazardous Materials, 180*(1–3), 332–339. http://dx.doi.org/10.1016/j.jhazmat.2010.04.035.

Hagler, G. S. W., Lin, M. Y., Khlystov, A., Baldauf, R. W., Isakov, V., Faircloth, J., et al. (2012). Field investigation of roadside vegetative and structural barrier impact on near-road ultrafine particle concentrations under a variety of wind conditions. *Science of the Total Environment, 419*, 7–15. http://dx.doi.org/10.1016/j.scitotenv.2011.12.002.

Ivings, M. J., Jagger, S. F., Lea, C. J., & Weber, D. M. (2007). *Evaluating vapor dispersion models for safety analysis of LNG facilities*. Harpur Hill, Buxton: UK HSL (Health and Safety Laboratories).

Koopman, R. P., & Ermak, D. L. (2007). Lessons learned from LNG safety research. *Journal of Hazardous Materials, 140*(3), 412–428. http://dx.doi.org/10.1016/j.jhazmat.2006.10.042.

Koopman, R. P., Ermak, D. L., & Chan, S. T. (1989). A review of recent field-tests and mathematical-modeling of atmospheric dispersion of large spills of denser-than-air gases. *Atmospheric Environment, 23*(4), 731–745. http://dx.doi.org/10.1016/0004-6981(89)90475-7.

Launder, B. E., & Spalding, D. B. (1972). *Lectures in mathematical models of turbulence*. London, England: Academic Press.

LNG World Shipping. (2006). *LNG spill tests*. Livermore, CA: Lawrence Livermore National Lab.

Luketa-Hanlin, A. (2006). A review of large-scale LNG spills: experiments and modeling. *Journal of Hazardous Materials, 132*(2–3), 119–140. http://dx.doi.org/10.1016/j.jhazmat.2005.10.008.

Luketa-Hanlin, A., Koopman, R. P., & Ermak, D. L. (2007). On the application of computational fluid dynamics codes for liquefied natural gas dispersion. *Journal of Hazardous Materials, 140*(3), 504–517. http://dx.doi.org/10.1016/j.jhazmat.2006.10.023.

Nielsen, M. (1998). *Dense gas dispersion in the atmosphere*. Denmark: Risø National Laboratory.

Pitblado, R. M., & Woodward, J. L. (2011). Highlights of LNG risk technology. *Journal of Loss Prevention in the Process Industries, 24*(6), 827–836. http://dx.doi.org/10.1016/j.jlp.2011.06.009.

Pontiggia, M., Busini, V., Derudi, M., Alba, M., Scaioni, M., Rota, R., et al. (2010). Safety of LPG rail transportation in the perspective of the Viareggio accident. In *Paper presented at the European Safety and Reliability Annual Conference: ESREL 2010*.

Pontiggia, M., Busini, V., Gattuso, M., Uguccioni, G., & Rota, R. (2012). Consequences assessment of an accidental toxic gas release through a CFD tool: effect of the terrain and major obstacles. *Chemical Engineering Transactions, 26*, 537–542.

Pontiggia, M., Derudi, M., Busini, V., & Rota, R. (2009). Hazardous gas dispersion: a CFD model accounting for atmospheric stability classes. *Journal of Hazardous Materials, 171*(1–3), 739–747. http://dx.doi.org/10.1016/j.jhazmat.2009.06.064.

Pontiggia, M., Landucci, G., Busini, V., Derudi, M., Alba, M., Scaioni, M., et al. (2011). CFD model simulation of LPG dispersion in urban areas. *Atmospheric Environment, 45*(24), 3913–3923. http://dx.doi.org/10.1016/j.atmosenv.2011.04.071.

Scaperdas, A., & Hebden, C. R. (2003). *Source term modelling of releases within building complexes*. Great Britain. Sudbury (GB): HSE Books.

Tauseef, S. M., Rashtchian, D., & Abbasi, S. A. (2011). CFD-based simulation of dense gas dispersion in presence of obstacles. *Journal of Loss Prevention in the Process Industries, 24*(4), 371–376. http://dx.doi.org/10.1016/j.jlp.2011.01.014.

Witlox, H. W. M., Harper, M., & Pitblado, R. (2013). Validation of PHAST dispersion model as required for USA LNG siting applications. *Chemical Engineering Transactions, 31*, 49–54. http://dx.doi.org/10.3303/cet1331009.

Woodward, J. L., & Pitblado, R. M. (2010). *LNG risk-based safety; modeling and consequence analysis* (p. 374). Hoboken, NJ: John Wiley and Sons, Inc.

Zhang, C. N., Ning, P., & Ma, C. X. (2009). Numerical simulation of dense gas leakage in plateau city at complex terrain. *Wuhan Ligong Daxue Xuebao/Journal of Wuhan University of Technology, 31*(20).